Peng *et al. Soft Sci* 2023;3:36
DOI: 10.20517/ss.2023.28

Soft Science

Research Article

Open Access

Check for updates

A highly stretchable and sintering-free liquid metal composite conductor enabled by ferrofluid

Maoyu Peng[1,#], Biao Ma[2,#], Guoqiang Li[3], Yong Liu[1], Yang Zhang[4], Xing Ma[3,*], Sheng Yan[1,*]

[1]Institute for Advanced Study Shenzhen University, Shenzhen 518060, Guangdong, China.
[2]State Key Laboratory of Digital Medical Engineering, School of Biological Science and Medical Engineering, Southeast University, Nanjing 210096, Jiangsu, China.
[3]Sauvage Laboratory for Smart Materials, Harbin Institute of Technology (Shenzhen), Shenzhen 518055, Guangdong, China.
[4]School of Engineering, Macquarie University, Sydney, NSW 2109, Australia.
[#]The authors contributed equally.

[*]**Correspondence to:** Prof. Xing Ma, Sauvage Laboratory for Smart Materials, Harbin Institute of Technology (Shenzhen), Xueyuan Avenue, Shenzhen 518055, Guangdong, China. E-mail: maxing@hit.edu.cn; Prof. Sheng Yan, Institute for Advanced Study Shenzhen University, Nanhai Road, Shenzhen 518060, Guangdong, China. E-mail: shengyan@szu.edu.cn

How to cite this article: Peng M, Ma B, Li G, Liu Y, Zhang Y, Ma X, Yan S. A highly stretchable and sintering-free liquid metal composite conductor enabled by ferrofluid. *Soft Sci* 2023;3:36. https://dx.doi.org/10.20517/ss.2023.28

Received: 20 Jun 2023 **First Decision:**12 Jul 2023 **Revised:** 7 Aug 2023 **Accepted:** 17 Aug 2023 **Published:** 16 Oct 2023

Academic Editor: Chuanfei Guo **Copy Editor:** Pei-Yun Wang **Production Editor:** Pei-Yun Wang

Abstract

Stretchable and highly conductive elastomers with intrinsically deformable liquid metal (LM) fillers exhibit promising potential in soft electronics, wearables, human-machine interfaces, and soft robotics. However, conventional LM-elastomer (LME) conductors require a high loading ratio of LM and the post-sintering to rupture LM particles to achieve electric conductivity, which results in high LM consumption and process complexity. In this work, we presented a straightforward and post-sintering-free method that utilizes magnetic aggregation to fabricate stretchable LME conductors. This was achieved by dispersing LM ferrofluid into the elastomer precursor, followed by applying the magnetic field to induce the aggregation and interconnection of the LM ferrofluid particles to form conductive pathways. This method not only simplifies the preparation of initially conductive LME but also reduces the LM loading ratio. The resulting conductive LME composites show high stretchability (up to 650% strain), high conductance stability, and magnetic responsiveness. The stretchable LME conductors were demonstrated in various applications, including the creation of flexible microcircuits, a magnetically controlled soft switch, and a soft hydrogel actuator for grasping tasks. We believe the stretchable LME conductors may find wide applications in electronic skins, soft sensors, and soft machines.

Keywords: Liquid metal, sintering-free, conductor, ferrofluid

INTRODUCTION

Soft and stretchable electronics that can conformably deform with nonplanar and dynamically moving surfaces hold great promise in various fields, such as wearable devices, soft robotics, and implantable devices[1-7]. Stretchable conductors with high conductivity are the basic building blocks for high-performance stretchable electronic devices[8]. Among various conductive materials designed for stretchable conductors[8,9], metals are quite attractive due to their merits of high electric conductivity, high thermal conductivity, and good stability. However, conventional solid metals can not withstand large deformation since they are rigid and brittle. To endow metal conductors with stretchability, conductive elastomeric composites with metal particle fillers[10,11] and rational structure design[12] (e.g., serpentine circuits, mesh structures, microcracks) have been frequently employed. However, the preparation of structure-based stretchable conductors involved complicated and costly metal deposition and microfabrication processes such as photolithography[8]. Although stretchable metal-elastomer composites show the advantages of ease of processing, printability, and high durability[13], a high concentration of rigid metallic particles is required to form percolated conducting pathways[14]. This could lead to the degradation of the mechanical properties of the composite by increasing its stiffness or tensile modulus[15]. In addition, since solid metals can not conformally deform with the elastomer, the separation of the metal particles poses a challenge to maintaining the conductance stability of the composite when stretched[16].

Gallium-based liquid metals (LMs) have emerged as attractive conductive fillers for stretchable conductors due to their excellent metal conductivity, inherent stretchability/deformability, self-healing ability, and neglected toxicity[17-24]. Unlike solid metal fillers, the fluidic LM particles can be deformed along the stretched matrix and maintain conductance stability[25]. However, most reported LM-elastomer (LME) composites are initially insulators and require an additional sintering process to realize electrical conductivity by rupturing the LM particles for electric connection[16,26-28]. To date, various post-sintering methods have been reported, such as mechanical pressing[16,29], freezing[30], and laser activation[31]. However, a high volume of LM addition (~50%) is required for sintering strategies, thus greatly increasing the composite density and leading to material waste[26]. Besides, new conductive pathways could also be activated during long-term use, which may induce the short-circuit issue[32]. Moreover, mechanical sintering may induce structure damage in delicate circuits, which is also not applicable to high-resolution circuits with microscale line widths[33]. Therefore, new strategies without post-sintering are highly needed for the fabrication of initially conductive LME composites.

In this article, we report a post-sintering-free method to create initially conductive LME composites by magnetic manipulation. This was achieved by dispersing LM ferrofluid into the elastomer. We show that continuous conductive pathways can be formed by applying the magnetic field to induce the magnetic aggregation and interconnection of the LM ferrofluid particles. This sintering-free method also offers several distinct advantages: (i) simple and low-cost preparation in an equipment-free manner; (ii) noncontact activation of the conductive pathways without damaging the circuits; (iii) being compatible with microscale circuits; (iv) enabling the composite with magnetic responsiveness; (v) without high loading of LM. In addition, the resulting LME composite shows high stretchability (~650% strain) and high electromechanical stability. We also demonstrated the applications of stretchable and responsive LME conductors in stretchable circuits, flexible magnetic switches, and soft hydrogel actuators.

EXPERIMENTAL

Chemicals and materials

The gallium and indium were purchased from Shanghai Macklin Biochemical Co., Ltd, Shanghai, China. The eutectic gallium-indium alloy (EGaIn) was prepared by heating the gallium and indium with a mass

ratio of 3:1 (75 g gallium and 25 g indium). Two elastomers of Ecoflex (Ecoflex 0030, Smooth-on, USA) and PDMS (Sylgard 184, Dow-Corning, USA) were used in this work. N-Isopropylacrylamide monomer [NIPAM, 98%, stabilized with hydroquinone methyl ether (MEHQ)] was purchased from Aladdin (Shanghai, China). Dimethylaminoethyl methacrylate (DMAEMA, 98.5%, stabilized with MEHQ) was supplied by TCI (Shanghai, China). Hydrolyzed poly(vinyl alcohol) (PVA124, 99%, MW ~105 kDa), poly(sodium-p-styrene sulfonate) (PSS, 98%, MW ~100 kDa), and ammonium persulfate (APS, 98%) were purchased from Sinopharm Chemical Reagent Beijing Co. Tetramethylethylenediamine (TEMED, 98%) and 7-hydroxy-4-methyl coumarin (98%) were supplied by J&K (Beijing, China).

Preparation of the LME composite

To prepare the LM ferrofluid, 2.8 g of Cu@Fe particles, 1 mL of EGaIn (~6.8 g), and 4.0 mL of the hydrochloric (HCl) solution were added into a clean beaker and stirred at 600 rpm to disperse Cu@Fe particles into EGaIn. To prepare the composite, 9.0 g of LM ferrofluid and 3.0 g of Ecoflex 0030 A were added into a beaker. Then, an electric stirrer equipped with a 4.0 mm diameter plastic stirring paddle was used to mix two parts at 500 rpm for 8 min. Then, 3.0 g Ecoflex 0030 B was added, and another 2 min mixing was required. Next, the mixture was poured into a plastic petri dish with a diameter of 6 mm and was degassed in a vacuum chamber for 5 min to remove air bubbles. Finally, the plastic petri dish was placed above the magnet for 5 min. The matrix magnet consists of 25 small cube magnets (5 mm × 5 mm × 5 mm) with N poles and S poles alternately arranged into a 5 × 5 square shape. Finally, the composite solution was cured at 60 °C for 30 min.

Preparation of the hydrogel actuator

The bilayer hydrogels were prepared in two simple stages. Free radical polymerization was used to create the initial layer of the PNIPAM/PVA hydrogel. Specifically, the NIPAM was added to the PVA solution (5 wt%), followed by adding the poly(ethylene glycol) diacrylate crosslinker with stirring for 30 min. Then, the initiator APS solution (30 mg/mL) and TEMED were added. The solution was quickly pumped into the glass cell with a rubber spacer (0.5 mm in thickness). To prepare the PNIPAM/PVA semi-IPN hydrogel, polymerization was carried out at 4 °C for 6 h. The second layer of the PDMAEMA/PSS hydrogel was synthesized by injecting DMAEMA pre-gel solution consisting of polymerizable monomer DMAEMA, PSS aqueous solution (10 wt%), and APS into the glass cell with a spacer thickness of 1.0 mm. The curing of the second layer was conducted at 20 °C for 6 h, accompanied by the reactive solution penetrating the surface of the first PNIPAM/PVA layer to create a strong adhesion between the two layers. To make it easier to peel off the composite layer, the upper glass substrate was covered with a hydrophobic PDMS membrane.

Characterization

The resistance of the LME composite was measured by a digital multimeter (Keithley DMM6500). The surface temperature of the hydrogel actuator was captured by a near-infrared camera (FLIR ONE Pro). Scanning electron microscopy (SEM) images and energy dispersive spectroscopy (EDS) mapping characterizations were taken using the Phenom XL. The micro-CT photos were taken using the ZEISS-Metrotom micro-CT tomography system.

RESULTS AND DISCUSSION

Preparation and mechanism of conductive LME without sintering

We reported a universal synthetic method of magnetic aggregation to create highly conductive LME without post-sintering. Unlike conventional LME, which uses pure LM particles as the conductive filler and requires the sintering to form conductive pathways [Figure 1A], we use the LM ferrofluid as the filler for magnetic manipulation of the LM particles to achieve electric conductivity. The LM ferrofluid was prepared by mixing Cu@Fe microparticles (~10 μm in diameter) with EGaIn in the HCl solution [Figure 1B and Supplementary Table 1]. The SEM and EDS images of the Cu@Fe microparticles are shown in

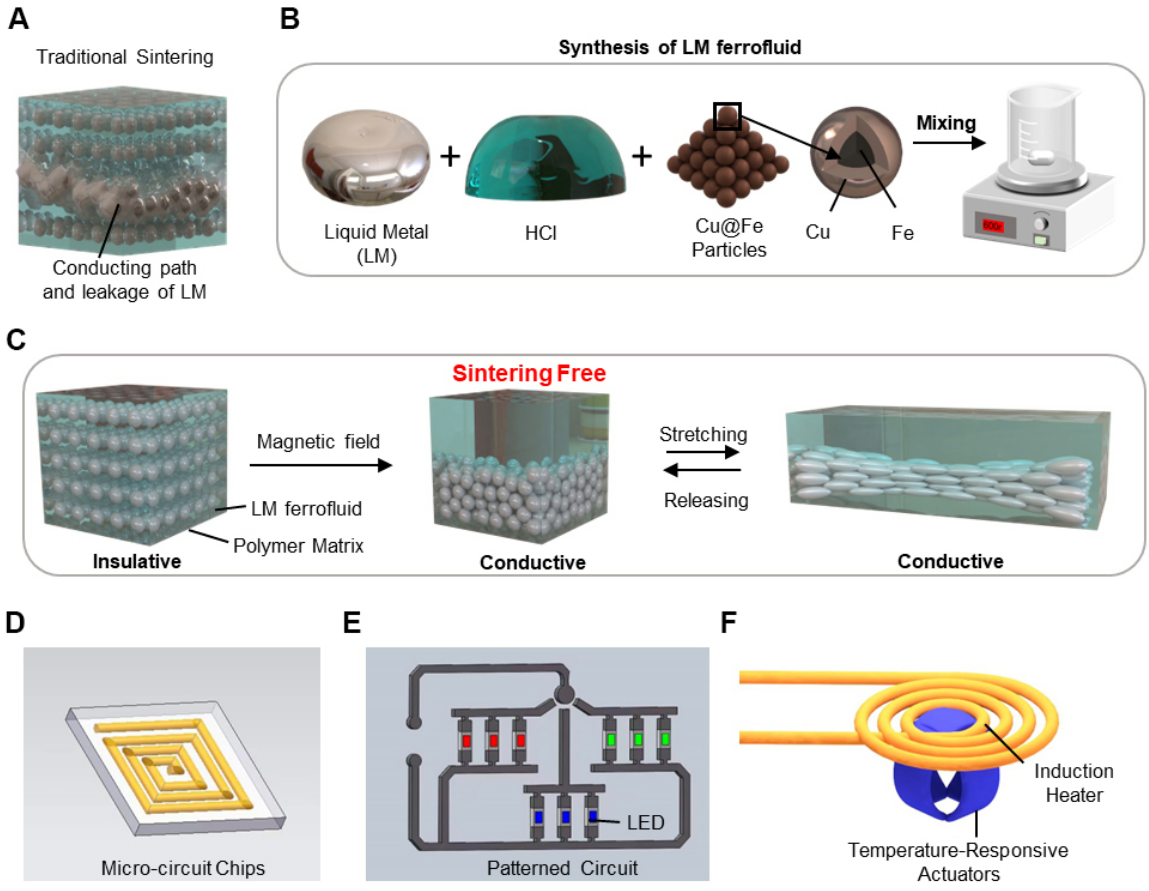

Figure 1. (A) The schematic of the conductive composite by a traditional sintering method; (B) The preparation process of the LM ferrofluid; (C) The schematic of the magnetic aggregation to create highly stretchable and conductive LME composites without post-sintering. The schematic of the micro-circuit chip (D), patterned circuit (E), and soft actuator (F) prepared by the LME composites. LM: Liquid metal; LME: LM-elastomer.

Supplementary Figure 1. The HCl solution was used to remove the oxidation layer of LM[34], allowing gallium to react with Cu to facilitate the dispersion of Fe particles into the LM. The chemical reaction between HCl and the oxide layer is $Ga_2O_3 + 6HCl \rightarrow 2GaCl_3 + 3H_2O$. We also characterized the Cu@Fe microparticles distributed near the LM surface by SEM. As shown in Supplementary Figure 2A, the Cu@Fe microparticles were fully wrapped by the LM due to the reactive wetting between Cu and Ga[35,36]. In contrast, the Fe particles tend to float on the LM surface with part of the particle not wetted by LM [Supplementary Figure 2B]. This result highlighted the importance of the use of Cu@Fe to facilitate the dispersion of Fe microparticles into the LM.

It should be noted that the diluted HCl does not react with copper since copper is below hydrogen in the reactivity series. Although the HCl solution can react with gallium with the formation of $GaCl_3$[37], the time for the acid treatment is short (~3 min), and the $GaCl_3$ is soluble in the aqueous solution. Thus, the reaction did not result in the contamination of LM. Other acids, such as sulfuric acid and nitric acid, could dissolve copper; thus, we did not choose these acid reagents. We also tried the weak acid of acetic acid, but this acid failed to facilitate the dispersion of Cu@Fe particles into LM.

The mechanism of conductive pathway formation in the magnetic LME is shown in Figure 1C. Initially, the LM ferrofluid microparticles are evenly distributed in the elastomer precursor solution. Under the magnetic field, the LM ferrofluid particles aggregate to connect to form continuous conductive networks at the composite bottom. We then cured the elastomer to form an initially conductive LME that can maintain high conductance stability when stretched.

The magnetic LME composites also show printability, allowing us to print various functional electronic components, such as micro-circuit chips [Figure 1D], patterned stretchable circuits [Figure 1E], and multilayer circuits. Furthermore, owing to the excellent thermal conductivity and thermal stability of the LM ferrofluid, the conductive LME composite can be embedded in temperature-responsive hydrogel actuators to achieve wireless induction heating [Figure 1F].

Preparation and characterization of conductive LME composite

The preparation of the conductive LME composite is schematically depicted in Figure 2A, and the details are provided in the Experimental Section and Supplementary Table 1. In a typical operation, we dispersed the LM ferrofluid to the Ecoflex 0030 part A by mechanical stirring. We observed the solution changed from colorless to opaque grey-black during the stirring. This is due to the formation of LM ferrofluid particles under the shear force. After mixing with the Ecoflex 0030 part B, we applied the magnetic field to the solution to attract LM ferrofluid microparticles to the composite bottom [Figure 2B]. The magnetic aggregation can increase the local concentration of LM ferrofluid particles and reduce the distance between the particles. Therefore, the LM ferrofluid particles tend to connect to form continuous conductive networks.

We also found the LM ferrofluid cannot maintain its ellipsoidal shape compared to the pure LM [Figure 2C and Supplementary Figure 3A]. To further explore the properties of the LM ferrofluid, we performed the contact angle and surface tension tests [Supplementary Figure 3B]. The results show that the contact angle and the surface tension of the LM ferrofluid were lower than those of the pure LM [Figure 2D]. We also compared the particle distribution in the composite before and after applying the magnetic field. For the composite without applying the magnetic field, the LM ferrofluid microparticles are uniformly dispersed in the elastomer matrix [Supplementary Figure 4]. For the one with magnetic aggregation, the composite exhibits the Janus structure with high stretchability [Figure 2E and F]: the upper insulative layer was in light grey with a low concentration of LM particles, while the lower conductive layer was grey and black with highly condensed magnetic LM particles.

Under the magnetic field, the LM ferrofluid microparticles aggregated at the bottom of the elastomer matrix. Since LM ferrofluid particles are almost incompressible, the magnetic force induces the LM ferrofluid droplets to merge by breaking the oxide layer of the LM [Supplementary Figure 5]. The SEM image shows the distribution of LM ferrofluid particles is increased from the top to the bottom, and the particles coalesce into a continuous conductive pathway at the bottom [Figure 2G]. We also used 3D micro-CT tomography to study the microstructure of the composite. We found that the denser LM ferrofluid droplets were aggregated at the bottom while the low-density elastomer matrix was concentrated at the top [Figure 2H]. SEM and corresponding EDS analysis further show that Cu@Fe microparticles were wrapped by LM in the composite [Figure 2I and J]. Our proposed magnetic aggregation method can activate the conductive filler networks before the elastomer curing without the post-sintering operation. Therefore, this approach can overcome the limitations of mechanical sintering on the hardness of the matrix, as the soft elastomer matrix (Ecoflex) cannot provide strong mechanical support for sintering.

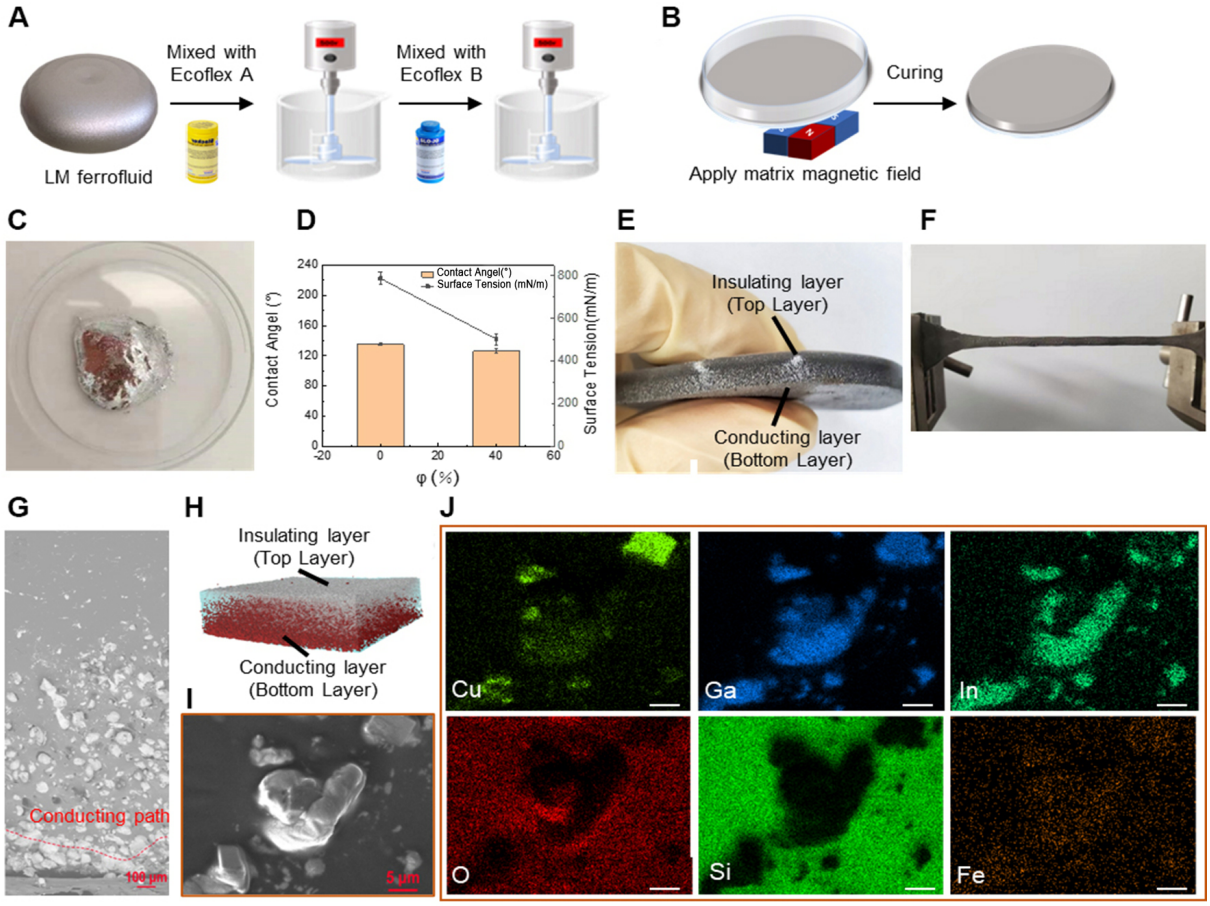

Figure 2. (A) Schematic of the preparation of the conductive LME composite; (B) Schematic of magnetic aggregation for connection of the LM ferrofluid particles; (C) The photograph of the LM ferrofluid; (D) The contact angle and surface tension when the Cu@Fe particles are at mass ratios of 0% and 40%; (E) The photograph of the conductive LME composite with a Janus structure; (F) The elongated state of the LME composite; (G) SEM image of the cross-section of the LME composite, the density of LM ferrofluid droplets is increased from top to bottom due to the applied magnetic field; (H) 3D micro-CT image of the LME composite. The red particles represent high-density LM ferrofluid particles, and the white particles represent low-density Ecoflex; (I) Cross-section SEM images of the LME conductive composite; (J) Element mappings of LME composite surface. LM: Liquid metal; LME: LM-elastomer; SEM: Scanning electron microscopy.

We also investigated the effect of the mass ratio of the conductive filler on the composite conductivity, as shown in Supplementary Figures 6 and 7. When the filler is the LM ferrofluid, the LME composite becomes conductive when the mass ratio of LM ferrofluid is 80%. When we replaced the filler with pure LM, we found that the composite was not conductive even though the mass ratio of LM reached 200%. Note that we performed the electric measurements by connecting the composite bottom with copper tape [Supplementary Figure 8]. Supplementary Table 2 compares the stretchability and the mass ratio of LM of our LME composite with other previously reported LM composites. Our LME composite initially shows conductivity at a low mass ratio of LM and has better stretchability than most of the reported composites. The small amount of LM ferrofluid required in conductive LME composite results in a reduction in the material density, which is of great interest in the preparation of lightweight and stretchable conductors.

For stretchable conductors, electromechanical performance is crucial for the reliability and stability of flexible devices. Figure 3A shows the results of the tensile tests of the three composites with LM ferrofluid, Cu@Fe, and Fe/LM fillers, respectively. The sample used for testing is shown in Supplementary Figure 9A,

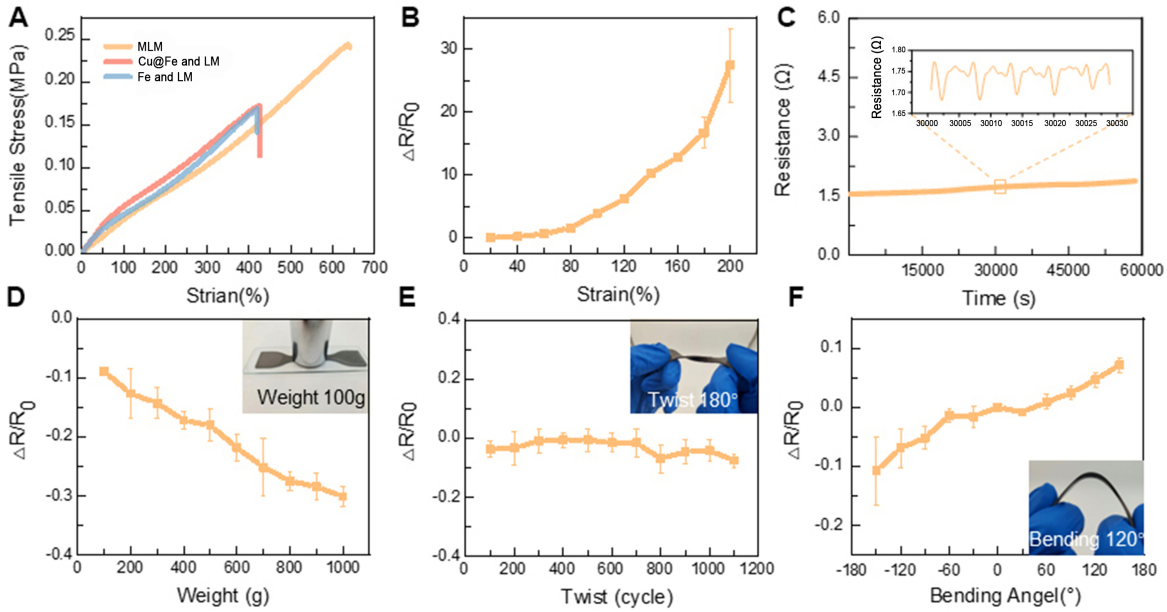

Figure 3. (A) The tensile stress-strain curves of the composites with Cu@Fe ferrofluid, the Cu@Fe/LM, and the Fe/LM fillers; (B) The relative resistance change of the composite under 200% tensile strain; (C) Cycling stability test under repeated 100% strain for 10,000 cycles of the LME composite; (D) The resistance change of LME composite under different weights from 0 to 1,000 g; (E) The resistance change of LME composite under repeated twisting 180° for 1,000 cycles; (F) The resistance change of LME conductive composite with different bending angles from -180° to 180°. LM: Liquid metal; LME: LM-elastomer.

and the schematic of the LM ferrofluid and Cu@Fe/LM fillers is shown in Supplementary Figure 9B. The composite with LM ferrofluid can reach ~650% strain until a mechanical failure is observed, which is higher than that of Cu@Fe/LM and Fe/LM fillers (~400%). In comparison with the smooth surface of conductive LME composite, there are a lot of bumps on the surfaces of composites with Cu@Fe/LM and Fe/LM fillers. These bumps are induced by the aggregation of the rigid metal particles when mixed with Ecoflex 0030, and they are more likely to produce defects during stretching and thus lead to fracture [Supplementary Figure 9C and D].

Figure 3B is the evolution of resistance change (R/R_0) of the conductive LME composite as a function of applied strain. The resistance change of LME composite under 200% strain is relatively stable, and the increased resistance might be attributed to the increased distance between the stretched LM ferrofluid particles. In addition, a 10,000-times long-term stability test was performed under 100% strain [Figure 3C]. The result demonstrates the high reliability of our conductive LME composite (resistance change between 1.5-1.9 Ω). Besides, we tested the electromechanical performance under compression. As shown in Figure 3D, the resistance change is negligible for 0-1,000 g loading weights. Figure 3E shows the result of stable resistance change (below 5%) of LME conductive composite under 1,000 times twisting test with 180. For the bending test, the resistance of the LME composite can remain stable with 180° forward and reverse bending [Figure 3F]. Overall, the multiple electromechanical tests demonstrated the outstanding electromechanical performance of the conductive LME composite.

Patterning of LME composite-based circuits

The conductive LME composite with good electromechanical properties is a competitive candidate for fabricating stretchable electric circuits. To form patterned functional circuits, we filled the composite solution into the grooves of a 3D-printed mold, followed by applying the magnetic field to create the

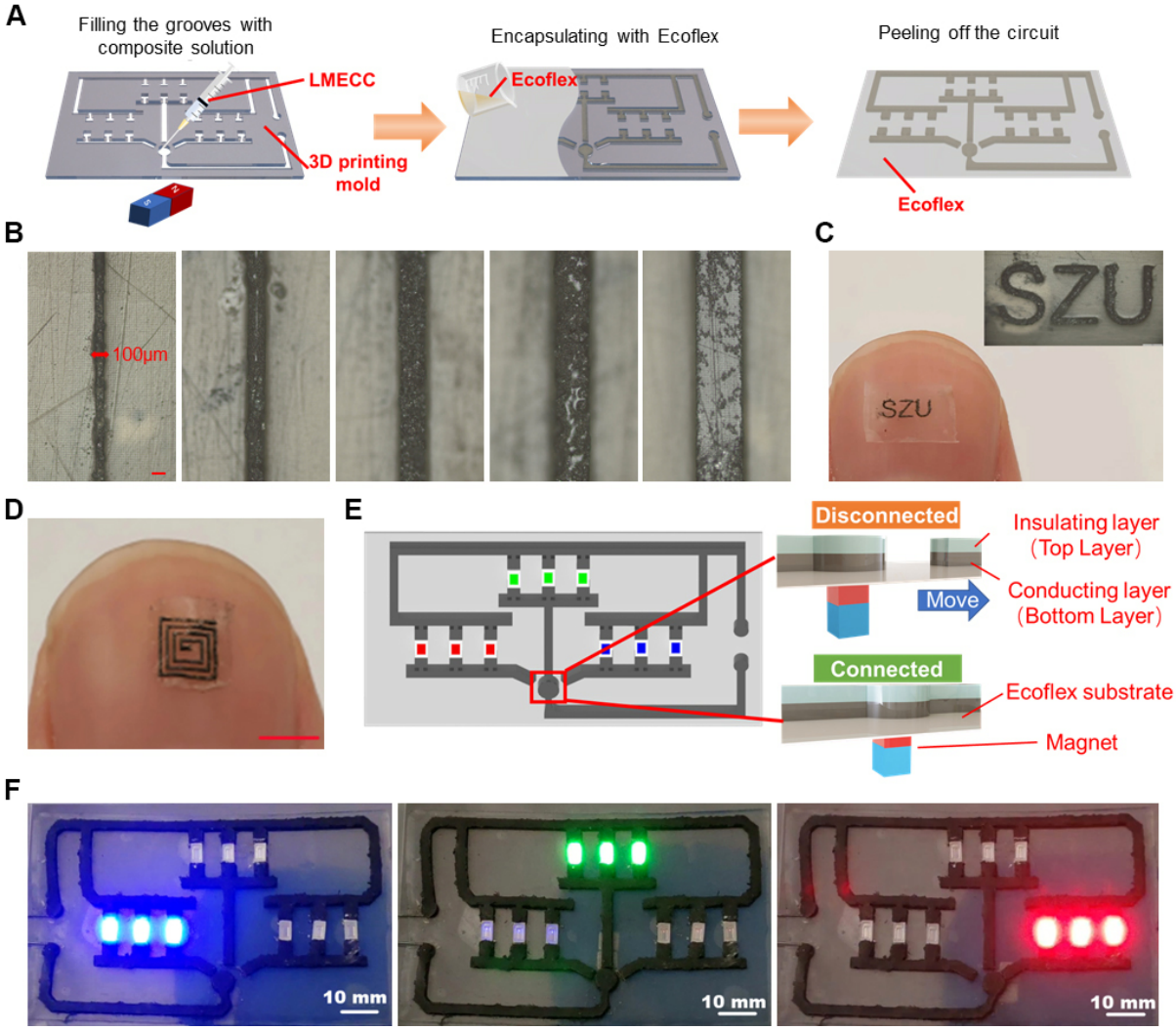

Figure 4. (A) Schematic of the preparation of the flexible LED circuit with magnetic LME composite as the switch; (B) Microscopic images of the LME circuits replicated with different linewidths (100, 200, 300, 400, and 500 μm). Scale bar: 100 μm; (C) Optical image and microscope image of the SZU logo. Scale bar: 3 mm; (D) Photographs of the prepared NFC antenna. Scale bar: 3 mm; (E) Schematic diagram showing the magnetic connection of the LME composite in the LED circuit; (F) Lighted LEDs in different connected ways. LME: LM-elastomer.

conductive networks [Figure 4A]. Then, a thin layer of Ecoflex 0030 was used to encapsulate the circuits. After curing, the conductive circuits and the encapsulation layer were peeled off from the mold. Using this method, the minimum linewidth of ~100 m [Figure 4B] was obtained, indicating the potential to create high-density stretchable circuits. Note that the minimum linewidth was limited by the resolution of the mold. We also created multiple flexible circuits, such as the "SZU" logo [Figure 4C] and an NFC antenna circuit [Figure 4D], and the line widths for the two circuits are 200 μm and 100 μm, respectively.

Furthermore, the LM ferrofluid also enables the conductive LME composite with magnetic responsiveness. As shown in Figure 4E, we designed a three-channel flexible circuit board with integrated LME composite as the magnetic switch. The LME composite can be manipulated by the magnet underneath to achieve the electric connection in a contactless manner [Figure 4F]. In addition, the Janus structure of the composite can also be used to create multilayer circuits. As shown in Supplementary Figure 10, the LED array is a double-layer circuit with several cross points. A strip-like LME composite Janus film can be easily stacked

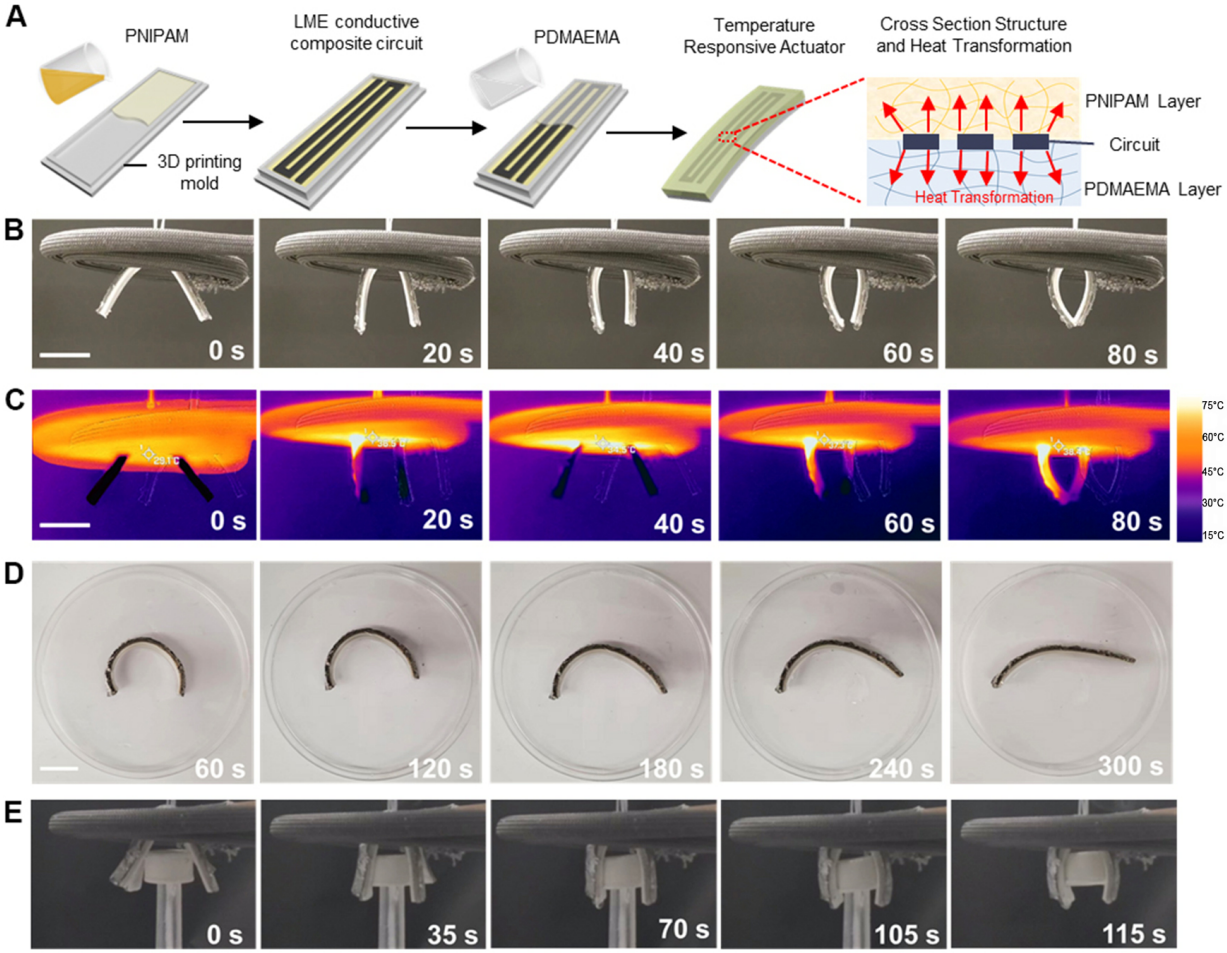

Figure 5. (A) Schematic illustration of the preparation of the hydrogel gripper; (B) and (C) Photographs and thermograms of the actuator with two-arm bending into a ring under the alternating magnetic heater for 80 s. Scale bar: 20 mm; (D) Photographs of the bilayer hydrogel recovering its shape at room temperature for 300 s. Scale bar, 15 mm; (E) Photographs of bilayer hydrogel as a four-arm gripper to capture the weight. Scale bar: 10 mm. LME: LM-elastomer.

without causing short-circuit. For homogeneous conductors, an insulation layer between the conductors is needed to form multilayer circuits.

LME composite-enabled hydrogel actuators

Soft actuators with high mechanical compliance show promising applications in soft machines[38,39]. The deformation of soft hydrogel actuators frequently relies on the changes in ambient temperature or the input current to the embedded heater, which is limited in multiple and complicated applications. Here, we optimized the hydrogel actuators by sandwiching the LME composite with the two layers of hydrogels. The soft hydrogel actuator can be actively controlled by the heat generated from the wirelessly electromagnetic field. Figure 5A illustrates the preparation of the hydrogel actuator. The mixture of NIPAM and PVA solution was added into a square-fluted mold and polymerized at 4 °C for 6 h to produce PNIPAM/PVA semi-interpenetrating networks. Then, the LME composite was placed on the PNIPAM/PVA hydrogel surface. The second layer of hydrogel was synthesized by injecting the DMAEMA pre-gel solution into the mold, followed by curing at 4 °C for 6 h for cross-linking with the PNIPAM/PVA hydrogel layer. Applied with the electromagnetic field, the hydrogel actuator with the two-armed structure can be actuated by the heat generated from numerous small eddy currents within the LM ferrofluid particles. As shown in

Figure 5B and C, we found that the surface temperature of the hydrogel can reach 60 °C, which is higher than the critical solution temperature (LCST) of 37 °C of PNIPAM. As a result, the PNIPAM layer will dehydrate and shrink and thus induce the bending motion [Figure 5B]. Finally, the two arms of the actuator will touch with each other and form a closed loop at 80 s. Besides, the recovery behavior of the actuator in alkaline solutions is shown in Figure 5D. Both PNIPAM and PDMAEMA have a high swelling rate at low temperatures, but the LCST of PDMAEMA decreases at higher pH values, i.e., with increasing OH^- concentrations, PDMAEMA shows a lower swelling while the PNIPAM layer does not have a pH response. Therefore, in a low-temperature alkaline environment, the swelling performance of the PNIPMA layer is more remarkable than that of the PDMAEMA layer, which can promote a faster recovery of the bilayer hydrogel to its original shape. For our actuator, the bilayer hydrogel takes about 300 s to recover to its starting state. In Figure 5E, we fabricated a four-arm gripper that can be actuated to bend towards the PNIPMA side under the alternating magnetic field for 115 s. The actuator can catch a 3 g bottle cap. Compared with the reported hydrogel actuators actuated by the direct current[40], our LME composite-based hydrogel actuators can be controlled wirelessly by the applied electromagnetic field in an untethered manner.

CONCLUSION

In this work, we proposed a simple yet efficient method of magnetic aggregation to fabricate initially conductive LME with high stretchability, conductance stability, printability, and magnetic responsiveness. This method allows the LM ferrofluid microparticles to be aggregated to form conductive networks in the bottom of the elastomer. Compared to the traditional preparation methods for conductive LME composites, our method does not require any post-sintering step that simplifies the preparation process. In addition, this method also reduces the consumption of LM, which benefits the creation of lightweight and low-cost stretchable LM conductors. We also demonstrated the applications of the initially conductive LME composite in high-resolution circuits, magnetically controllable switches, and thermally responsive soft hydrogel actuators. We believe these stretchable LME conductors may find wide applications in stretchable electronic devices, soft robotics, and intelligent human-machine interactions.

DECLARATIONS

Authors' contributions

Data curation, formal analysis, investigation, methodology, writing original draft: Peng M, Li G, Ma B, Liu Y, Zhang Y
Conceptualization: Yan S, Ma X
Methodology: Peng M, Li G, Ma B, Liu Y, Zhang Y
Visualization: Peng M, Ma B, Li G
Data analysis: Peng M, Li G, Ma B, Liu Y
Data curation, formal analysis, and supervision: Peng M, Li G, Ma B
Conceptualization, funding acquisition, project administration, resources, supervision and writing, review and editing: Yan S, Ma X

Availability of data and materials

Not applicable.

Financial support and sponsorship

Yan S thanks for the financial support from the Guangdong Basic and Applied Basic Research Foundation (2021A1515110277 and 2021QN02Y387) and the Shenzhen Natural Science Fund (20200811205344001).

Conflicts of interest

All authors declared that there are no conflicts of interest.

Ethical approval and consent to participate

Not applicable.

Consent for publication

Not applicable.

Copyright

REFERENCES

1. Rogers JA, Someya T, Huang Y. Materials and mechanics for stretchable electronics. *Science* 2010;327:1603-7. DOI PubMed
2. Shim H, Sim K, Wang B, et al. Elastic integrated electronics based on a stretchable n-type elastomer-semiconductor-elastomer stack. *Nat Electron* 2023;6:349-59. DOI
3. Sun X, Wang X, Yuan B, Liu J. Liquid metal-enabled cybernetic electronics. *Mater Today Phys* 2020;14:100245. DOI
4. Zhang M, Wang X, Huang Z, Rao W. Liquid metal based flexible and implantable biosensors. *Biosensors* 2020;10:170. DOI PubMed PMC
5. Heng W, Solomon S, Gao W. Flexible electronics and devices as human-machine interfaces for medical robotics. *Adv Mater* 2022;34:e2107902. DOI PubMed PMC
6. Qu J, Pan H, Sun Y, Zhang H. Multitasking device regulated by the gravity field: broadband anapole-excited absorber and linear polarization converter. *Annalen der Physik* 2022;534:2200175. DOI
7. Wu F, Shi P, Yi Z, Li H, Yi Y. Ultra-broadband solar absorber and high-efficiency thermal emitter from UV to mid-infrared spectrum. *Micromachines* 2023;14:985. DOI PubMed PMC
8. Matsuhisa N, Chen X, Bao Z, Someya T. Materials and structural designs of stretchable conductors. *Chem Soc Rev* 2019;48:2946-66. DOI
9. Jiang Y, Wang Y, Mishra YK, Adelung R, Yang Y. Stretchable CNTs-Ecoflex composite as variable-transmittance skin for ultrasensitive strain sensing. *Adv Mater Technol* 2018;3:1800248. DOI
10. Kim DC, Shim HJ, Lee W, Koo JH, Kim DH. Material-based approaches for the fabrication of stretchable electronics. *Adv Mater* 2020;32:e1902743. DOI PubMed
11. Larmagnac A, Eggenberger S, Janossy H, Vörös J. Stretchable electronics based on Ag-PDMS composites. *Sci Rep* 2014;4:7254. DOI PubMed PMC
12. Kim DH, Lu N, Ma R, et al. Epidermal electronics. *Science* 2011;333:838-43. DOI
13. Lee P, Lee J, Lee H, et al. Highly stretchable and highly conductive metal electrode by very long metal nanowire percolation network. *Adv Mater* 2012;24:3326-32. DOI
14. Kim Y, Zhu J, Yeom B, et al. Stretchable nanoparticle conductors with self-organized conductive pathways. *Nature* 2013;500:59-63. DOI
15. Benli S, Yilmazer Ü, Pekel F, Özkar S. Effect of fillers on thermal and mechanical properties of polyurethane elastomer. *J Appl Polym Sci* 1998;68:1057-65. Available from: https://onlinelibrary.wiley.com/doi/10.1002/(SICI)1097-4628(19980516)68:7%3C1057::AID-APP3%3E3.0.CO;2-E. [Last accessed on 13 Oct 2023]
16. Boley JW, White EL, Kramer RK. Mechanically sintered gallium-indium nanoparticles. *Adv Mater* 2015;27:2355-60. DOI PubMed
17. Dickey MD. Stretchable and soft electronics using liquid metals. *Adv Mater* 2017;29:1606425. DOI PubMed
18. Khoshmanesh K, Tang SY, Zhu JY, et al. Liquid metal enabled microfluidics. *Lab Chip* 2017;17:974-93. DOI
19. Malakooti MH, Kazem N, Yan J, et al. Liquid metal supercooling for low-temperature thermoelectric wearables. *Adv Funct Mater* 2019;29:1906098. DOI
20. Paracha KN, Butt AD, Alghamdi AS, Babale SA, Soh PJ. Liquid metal antennas: materials, fabrication and applications. *Sensors* 2019;20:177. DOI PubMed PMC
21. Park YG, Lee GY, Jang J, Yun SM, Kim E, Park JU. Liquid metal-based soft electronics for wearable healthcare. *Adv Healthc Mater* 2021;10:2002280. DOI
22. Ren L, Zhang BW. Room temperature liquid metals for flexible alkali metal-chalcogen batteries. *Exploration* 2022;2:20210182. DOI PubMed PMC
23. Liu T, Zhuge X, Lan J, et al. Study on the 3D printing of flexible pressure sensor by using polyurethane pressure sensitive materials and encapsulated gainsn liquid metal wires. *Materials Reports* 2022;36:21030297-5. DOI
24. Jackson N, Buckley J, Clarke C, Stam F. Manufacturing methods of stretchable liquid metal-based antenna. *Microsyst Technol* 2019;25:3175-84. DOI
25. Fassler A, Majidi C. Liquid-phase metal inclusions for a conductive polymer composite. *Adv Mater* 2015;27:1928-32. DOI PubMed

26. Chen S, Wang H, Zhao R, Rao W, Liu J. Liquid metal composites. *Matter* 2020;2:1446-80. DOI
27. Liu S, Kim SY, Henry KE, Shah DS, Kramer-Bottiglio R. Printed and laser-activated liquid metal-elastomer conductors enabled by ethanol/PDMS/liquid metal double emulsions. *ACS Appl Mater Interfaces* 2021;13:28729-36. DOI PubMed
28. Pan C, Liu D, Ford MJ, Majidi C. Ultrastretchable, wearable triboelectric nanogenerator based on sedimented liquid metal elastomer composite. *Adv Mater Technol* 2020;5:2000754. DOI
29. Lin Y, Cooper C, Wang M, Adams JJ, Genzer J, Dickey MD. Handwritten, soft circuit boards and antennas using liquid metal nanoparticles. *Small* 2015;11:6397-403. DOI PubMed
30. Wang H, Yao Y, He Z, et al. A highly stretchable liquid metal polymer as reversible transitional insulator and conductor. *Adv Mater* 2019;31:e1901337. DOI
31. Liu S, Yuen MC, White EL, et al. Laser sintering of liquid metal nanoparticles for scalable manufacturing of soft and flexible electronics. *ACS Appl Mater Interfaces* 2018;10:28232-41. DOI
32. Yun G, Tang S, Lu H, Zhang S, Dickey MD, Li W. Hybrid-filler stretchable conductive composites: from fabrication to application. *Small Sci* 2021;1:2000080. DOI
33. Liu S, Xu Z, Li G, et al. Ultrasonic-enabled nondestructive and substrate-independent liquid metal ink sintering. *Adv Sci* 2023;10:e2301292. DOI PubMed PMC
34. Ren L, Sun S, Casillas-Garcia G, et al. A liquid-metal-based magnetoactive slurry for stimuli-responsive mechanically adaptive electrodes. *Adv Mater* 2018;30:1802595. DOI
35. Cui Y, Liang F, Yang Z, et al. Metallic bond-enabled wetting behavior at the liquid Ga/$CuGa_2$ interfaces. *ACS Appl Mater Interfaces* 2018;10:9203-10. DOI
36. Kim JH, Kim S, Kim H, et al. Imbibition-induced selective wetting of liquid metal. *Nat Commun* 2022;13:4763. DOI PubMed PMC
37. Handschuh-wang S, Chen Y, Zhu L, Zhou X. Analysis and transformations of room-temperature liquid metal interfaces - a closer look through interfacial tension. *ChemPhysChem* 2018;19:1551. DOI
38. Liu D, Liu X, Chen Z, et al. Magnetically driven soft continuum microrobot for intravascular operations in microscale. *Cyborg Bionic Syst* 2022;2022:9850832. DOI PubMed PMC
39. Zheng Y, Yi Z, Liu L, et al. Numerical simulation of efficient solar absorbers and thermal emitters based on multilayer nanodisk arrays. *Appl Therm Eng* 2023;230:120841. DOI
40. Mao G, Drack M, Karami-Mosammam M, et al. Soft electromagnetic actuators. *Sci Adv* 2020;6:eabc0251. DOI PubMed PMC